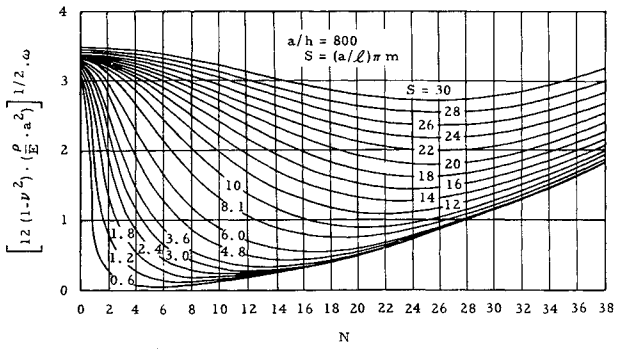

Fig. 5 Natural frequency of cylindrical shells.

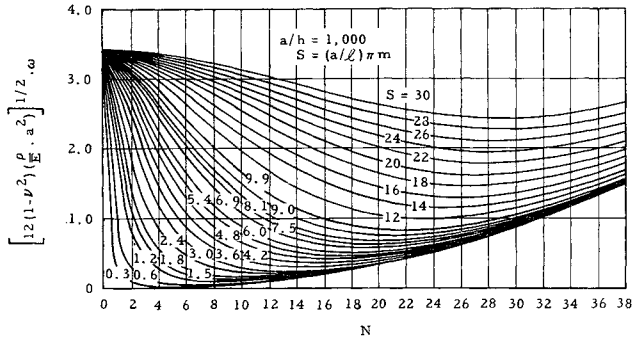

Fig. 6 Natural frequency of cylindrical shells.

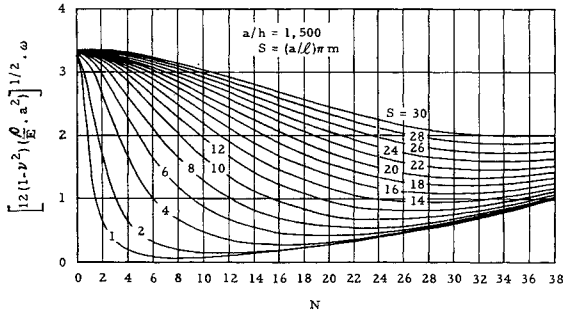

Fig. 7 Natural frequency of cylindrical shells.

where $s = ma\pi/l$. The cylinder length is l, and m is the number of half-waves in the x direction. Combining Eqs. (1) and (2) yields the following frequency equation:

$$\left\{\left[12(1-\nu^2)\cdot\left(\frac{\rho}{E}\right)\right]\cdot a^2\right\}^{1/2}\cdot\omega_{sn} = \frac{h/a}{s^2+n^2}\times [(s^2+n^2)^2(s^2+n^2-1)^2+4K^4s^4]^{1/2} \quad (3)$$

Charts based on Eq. (3) are prepared with

$$\left[12(1-\nu^2)\,\frac{\rho}{E}\,a^2\right]^{1/2}\omega_{sn}$$

as the frequency parameter; shown in Figs. 1–7. It is believed that the range of the curves thus covered is broad enough for engineering uses.

References

[1] Weingarten, V. I., "Free vibration of thin cylindrical shells," AIAA J. 2, 717–722 (1964).

[2] Morley, L. S. D., "An improvement on Donnell's approximation for thin-walled circular cylinders," Quart. J. Mech. Appl. Math. XII, 93 (1959).

Separated Flow Behind a Rearward-Facing Step with and without Combustion

J. M. Bowyer Jr.* and W. V. Carter†
General Dynamics/Astronautics, SanDiego, Calif.

Introduction

Reduction of the transonic and low supersonic base drag of aircraft designed to operate efficiently at hypersonic speeds has become an important goal in recent years. Base drag is an important component of the total drag of such aircraft because, typically, optimum hypersonic bodies have slender, pointed forebodies and blunt afterbodies. One scheme that has been proposed as a means for reducing the base drag of hypersonic vehicles traveling at transonic and moderate supersonic speeds is to inject fuel into the region of separated flow at the base and to burn this fuel in the free boundary layer separating the base flow from the main stream. The experimental program reported here was devised to allow the study of a closely related problem, viz., the problem of the separated flow field behind a rearward-facing step with and without hydrogen combustion in the separated region. Experimental results are compared with corresponding predictions of an approximate analytic model.

Description of the Model and Its Instrumentation

A simplified vertical center plane sectional drawing of the model is presented in Fig. 1. A two-dimensional, convergent-divergent half-nozzle was designed by the method of characteristics to provide a uniform, supersonic ($M \approx 1.5$) air stream to the upstream side of a rearward-facing step. This half-nozzle has a constant width of 6 in. The height of the nozzle entry section is 3 in., of the throat, 1 in., and of the exit, 1.23 in. (including an allowance for the development of a turbulent boundary layer downstream of the throat of the half-nozzle). The upper surface of the half-nozzle is contoured; the lower surface is plane. A $\frac{1}{2}$-in.-deep by 6-in.-wide rearward-facing step is formed by a $\frac{1}{2}$-in. offset of the duct wall at the exit plane and on the contoured (upper) side of the half-nozzle. A $\frac{1}{16}$-in.-high slot spans the rearward-facing plane surface (riser) of the step at a distance of $\frac{1}{16}$in. from the outside corner of the step. This slot allows hydrogen (from the 4-in. central section of the plenum) and cooling air for the side glasses (from the two 1-in. side sections of the plenum) to be injected in a direction that is, as nearly as possible, parallel to the direction of and contiguous to the main air flow at the nozzle exit. The side walls of the nozzle are steel to a station located about $\frac{1}{2}$in. upstream from the nozzle exit. Plate glass windows, 1in. thick, extend the side walls from this station to a station about 9 in. further downstream. These glass side

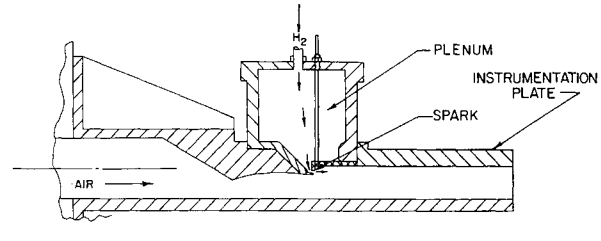

Fig. 1 Vertical center plane section of the model.

Received July 30, 1963; revision received October 7, 1964.

* Senior Staff Scientist, Space Science Laboratory; now Associate Professor of Mechanical Engineering, Kansas State University. Associate Fellow Member AIAA.

† Design Specialist. Member AIAA.

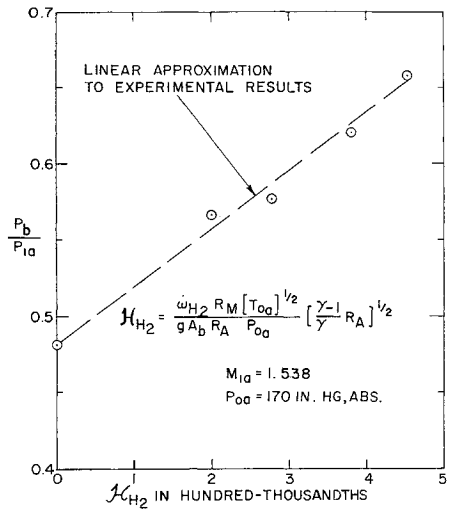

Fig. 2 Base pressure ratio as a function of dimensionless mass base bleed rate.

walls were incorporated to allow schlieren, shadowgraphic, and ordinary visual observation of the flow in the step region.

A water-cooled instrumentation plate extends approximately 11 in. downstream from the rearward-facing step. The instrumentation installed in this plate consists of pressure orifices, thermocouples, and calorimeters. This instrumentation is mounted flush with the plate surface.

Discussion of Tests

In order to verify that the boundary layer as it separated from the step was, in fact, thin and fully turbulent at separation, the no-bleed base pressure was plotted as a function of Reynolds number (based on freestream conditions at the step and step height) on log-log paper. The slope of the straight line fitted to these data is very nearly minus $\frac{1}{5}$, and this relationship between pressure ratio and Reynolds number is typical of turbulent boundary-layer separation or reattachment.

Once the existence of a thin turbulent free boundary layer was confirmed, the next step taken in analyzing the experimental data was to plot base pressure ratio as a function of weight rate of hydrogen bled into and burned in the base

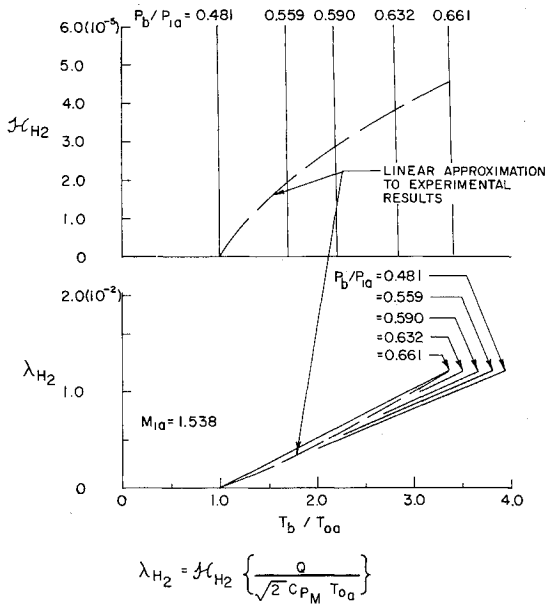

Fig. 3 Dimensionless mass and energy base bleed rates as functions of the base temperature ratio predicted by the method of Korst.

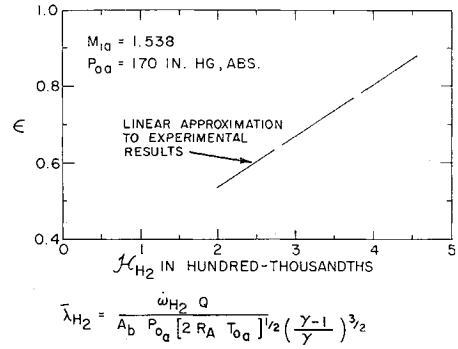

Fig. 4 Efficiency as a function of dimensionless mass base bleed rate.

region. Primary air supply stagnation pressure was employed as a parameter; however, only the results obtained for P_{0a} = 170 in. Hg absolute will be reported here. Similar results were obtained at P_{0a} = 111 in. Hg absolute. Experimental values of base pressure ratio p_b/p_{1a} are presented with corresponding experimental values of dimensionless mass base bleed rate $\mathcal{H}_{H_2}$ in Fig. 2.‡ A linear approximation to the experimental results is also presented in the same figure.

The results obtained by applying the approximate analytic model of Korst[1, 2] and the corresponding graphs of auxiliary integrals presented in Refs. 3 and 4 to the experimental case reported here are shown in Fig. 3. This figure presents dimensionless mass base bleed rate $\mathcal{H}_{H_2}$ and dimensionless energy base bleed rate λ_{H_2} (predicted by Korst's method of analysis) as functions of base temperature ratio T_b/T_{0a} for the linear approximation to each of the experimentally established base pressure ratios shown in Fig. 2.

The efficiency with which energy is added to the base region ϵ is defined here as the ratio of the dimensionless energy bleed rate determined from Korst's theory at a given value of $\mathcal{H}_{H_2}$ to the energy base bleed rate determined from experimental data at the same value of $\mathcal{H}_{H_2}$, i.e., $\epsilon = \lambda_{H_2}/\bar{\lambda}_{H_2}^{1/2}$. Efficiency is plotted as a function of $\mathcal{H}_{H_2}$ in Fig. 4. Obviously, efficiency must necessarily level off for flow rates higher than those employed, or a distinct fault in the data and/or the theoretical model of Korst would result.

The fuel specific impulse realized in the tests reported here was virtually constant at all nonzero rates of hydrogen base bleed: for $1.99(10^{-5}) \leq \mathcal{H}_{H_2} \leq 4.525(10^{-5})$, 15,000 sec $\leq I_{sp} \leq$ 16,000 sec.

Very shortly after the tests reported here were completed, the authors' attention was directed to a similar investigation that had just been reported by Townend and Reid.[5] Extrapolation of the results presented by Townend in Fig. 16 of Ref. 6 to values of dimensionless hydrogen mass flow corresponding to the dimensionless hydrogen base bleed rates employed in the tests reported here indicate that a hydrogen specific impulse of eighteen thousand might be achieved with Townend's model if combustion could have been maintained at such a small hydrogen flow. In actuality, Townend reported an inability to maintain hydrogen combustion in the base region of his model at a dimensionless hydrogen base bleed rate, $\mathcal{H}_{H_2}$ (as defined herein), of less than about $0.6(10^{-3})$. Townend's model was a side-strut-mounted cone-cylinder of 1-in. external diameter designed to minimize strut and tunnel interference effects.

Summary of Results

The evidence presented in this report indicates that, as a means for counteracting base drag on a blunt-based vehicle flying at a Mach number of $1\frac{1}{2}$, the burning of hydrogen in the base region is three to five times as effective as the burning

‡ Except as noted in the figures, the symbols employed in this discussion are identical with those employed in Refs. 1 and 2.

of additional hydrogen in the vehicle's primary propulsion system for base drag reductions of as much as $\frac{1}{2}$.

References

[1] Korst, H. H., "A theory for base pressures in transonic and supersonic flow," J. Appl. Mech. **23**, 593–600 (December 1956).

[2] Page, R. H. and Korst, H. H., "Nonisoenergetic turbulent compressible jet mixing with consideration of its influence on the base pressure problem," Transactions of the 4th Midwestern Conference on Fluid Mechanics, pp. 45–68 (September 1955).

[3] Korst, H. H. and Chow, W. L., "Compressible non-isoenergetic two-dimensional turbulent ($Pr_t = 1$) jet mixing at constant pressure—auxiliary integrals, heat transfer, and friction coefficients for fully developed mixing profiles," Univ. of Ill. Engineering Experiment Station, Mechanical Engineering Dept. TN 392–4 (January 1959).

[4] Korst, H. H., Graphs of auxiliary integrals for selected values of T_b/T_{0_a} from 4.0 to 10.0 and presented in a form similar to that of Ref. 3 were received from H. H. Korst through S. Stillwell (1961).

[5] Townend, L. H. and Reid, J., "Experimental results on the effect of combustion on base flows at supersonic speeds," (abstract of) NATO AGARD Combustion and Propulsion Panel Meeting on Supersonic Flow, Chemical Processes, and Radiative Transfer, Whitehall, London, England (April 1–5, 1963).

[6] Townend, L. H., "Some effects of stable combustion in wakes formed in a supersonic stream," Royal Aircraft Establishment (Farnborough) TN Aero. 2872, Ministry of Aviation, London (March 1963).

Measurements in a Free Piston Shock Tube

RALPH GREIF* AND ARTHUR E. BRYSON JR.†

Harvard University, Cambridge, Mass.

EXPERIMENTAL measurements have been obtained in a free piston shock tube. This shock tube uses a piston compression as the method for transferring energy to the driver gas.[1, 2] The piston is propelled by high pressure, and the compression process continues until the diaphragm is broken. The compressed driver gas then expands into the expansion section driving a shock wave down the length of the tube.

The passage of the shock wave was detected by thin film resistance gages that were mounted in the shock tube wall. These gages were made by Rolf W. F. Gross. The Mach number of the shock wave was obtained from the resulting distance vs time measurements. The diameter of the expansion tube

Table 1 Speed of reflected shock wave for helium

Incident shock wave	Ratio of speed of shock waves
M_s	$-U_R/U_S$
2.74	0.500
2.74	0.503
2.80	0.496
2.85	0.487
2.89	0.486
2.93	0.488
2.95	0.494

Received April 6, 1964; revision received September 24, 1964. This research was supported by a grant from the National Science Foundation to Harvard University. The authors wish to thank Barron C. Watson, Daniel J. Collins, Jan Rosciszewski, Rolf W. F. Gross, Jerry F. Bott, and Gordon Brownell for their assistance.

* Assistant Professor of Mechanical Engineering, University of California, Berkeley, Calif. Member AIAA.

† Professor of Mechanical Engineering. Associate Fellow Member AIAA.

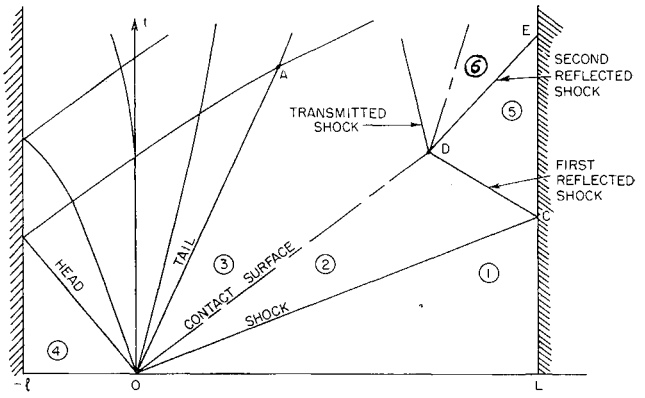

Fig. 1 Flow regimes in the shock tube.

affects the performance of the shock tube because of the growth of the boundary layer on the wall behind the shock wave.[3–5] The smaller the tube diameter, the greater the attenuation of the shock speed, and the shorter the testing time. Our experiments were performed in a 2-in.-diam expansion tube. For Mach numbers less than 6 in helium, the maximum shock wave attenuation was $1\frac{1}{2}\%$/ft length.

The speed of the reflected shock wave was obtained from the two successive signals produced by the thin film resistance gage nearest the end wall. The two signals correspond to the passage of the incident and the reflected shock wave, respectively. Knowing the distance between the gage and the end wall, we obtain the average speed of the two shock waves. Then, using the value for the speed of the incident shock wave, the speed of the reflected shock wave can be obtained. The results for helium are given in Table 1 and are in good agreement with those reported by Strehlow and Cohen[6] for argon. The theoretical values for the ratio $-U_R/U_S$ are bounded by

$$0.557 < -U_R/U_S < 0.567$$

for the Mach number range of Table 1.

The maximum available testing time in the region behind the first reflected shock wave, region 5 of Fig. 1, is also of interest. This is the time between the arrival of the incident shock wave at the end wall t_C and the arrival of the second reflected shock wave at the end wall t_E. The second reflected shock wave results from the interaction of the first reflected shock wave with the contact surface. The arrival times of these two shock waves were detected with a thin film re-

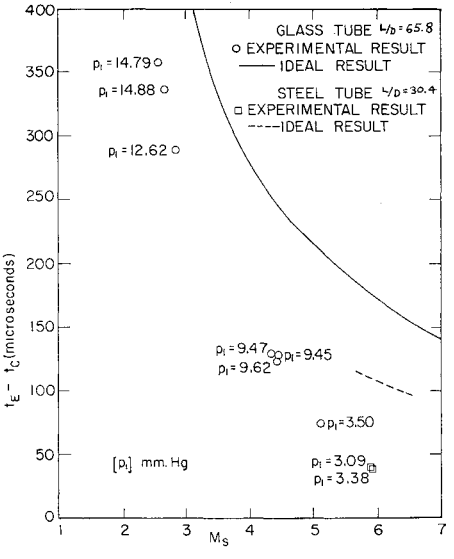

Fig. 2 Maximum testing time behind reflected shock wave.